Regio-selective Detection of Dynamic Structure of Transmembrane α-Helices as Revealed from ^{13}C NMR Spectra of [3-^{13}C]Ala-labeled Bacteriorhodopsin in the Presence of Mn^{2+} Ion

Satoru Tuzi, Jun Hasegawa, Ruriko Kawaminami, Akira Naito, and Hazime Saitô
Department of Life Science, Himeji Institute of Technology, Harima Science Garden City, Kouto 3-chome, Kamigori, Hyogo 678-1297, Japan

ABSTRACT ^{13}C Nuclear magnetic resonance (NMR) spectra of [3-^{13}C]Ala-labeled bacteriorhodopsin (bR) were edited to give rise to regio-selective signals from hydrophobic transmembrane α-helices by using NMR relaxation reagent, Mn^{2+} ion. As a result of selective suppression of ^{13}C NMR signals from the surfaces in the presence of Mn^{2+} ions, several ^{13}C NMR signals of Ala residues in the transmembrane α-helices were identified on the basis of site-directed mutagenesis without overlaps from ^{13}C NMR signals of residues located near the bilayer surfaces. The upper bound of the interatomic distances between ^{13}C nucleus in bR and Mn^{2+} ions bound to the hydrophilic surface to cause suppressed peaks by the presence of Mn^{2+} ion was estimated as 8.7 Å to result in the signal broadening to 100 Hz and consistent with the data based on experimental finding. The Ala C_β ^{13}C NMR peaks corresponding to Ala-51, Ala-53, Ala-81, Ala-84, and Ala-215 located around the extracellular half of the proton channel and Ala-184 located at the kink in the helix F were successfully identified on the basis of ^{13}C NMR spectra of bR in the presence of Mn^{2+} ion and site-directed replacement of Ala by Gly or Val. Utilizing these peaks as probes to observe local structure in the transmembrane α-helices, dynamic conformation of the extracellular half of bR at ambient temperature was examined, and the local structures of Ala-215 and 184 were compared with those elucidated at low temperature. Conformational changes in the transmembrane α-helices induced in D85N and E204Q and its long-range transmission from the proton release site to the site around the Schiff base in E204Q were also examined.

INTRODUCTION

Bacteriorhodopsin (bR) is a light-driven proton pump of archaebacteria, *Halobacterium salinarum*, which consists of seven transmembrane $\alpha-$helices, helix A to G, and a chromophore, retinal, covalently linked to Lys-216 in the helix G (Lanyi, 1993, 1997; Mathies et al., 1991; Ovchinnikov, 1982; Stoeckenius and Bogomolni, 1982). bR is known to be concentrated in the cell membrane of *H. salinarum* as a two-dimensional (2D) crystal patch named purple membrane consisting of bR and lipids. Recent x-ray diffraction studies revealed three-dimensional (3D) atomic coordinates with resolution up to 1.55 Å for bR at liquid nitrogen temperature (Edman et al., 1999; Luecke, 2000; Luecke et al., 1999ab; Sass et al., 2000). In addition to its own right as a proton pump, bR has been considered as a simple and convenient model system for a variety of membrane protein, which consists of transmembrane α-helical bundle, e.g., G-protein coupled receptor.

Solid-state nuclear magnetic resonance (NMR) spectroscopy, based on magnetically unoriented (Saitô et al., 1998; 2000) and oriented bilayer systems (Cross, 1997; Marassi and Opella, 1998), is certainly the most powerful means to reveal the dynamic structure of membrane proteins under physiological conditions. In particular, the former approach relies on the conformation-dependent displacements of ^{13}C NMR peaks of individual amino-acid residues depending on local conformation of a given peptide unit characterized by the torsion angles (ϕ and φ) irrespective of the peptide-sequence and can be considered as the only practical means to be able to study a whole protein system at present (Saitô et al., 2000). This approach has proved to be very useful for revealing secondary structures of globular or fibrous proteins in the solid state where no significant backbone motion is present (Saitô and Ando, 1989). On the contrary, polypeptide backbone from membrane proteins in lipid bilayers turned out to be far from a static picture at ambient temperature, but to be able to undergo sequence-specific motions ($>10^2$ Hz) (Kimura et al., 2001) or intermediate motion (10^4–10^5 Hz) to result in dynamically averaged chemical shift of ^{13}C NMR signals (Tuzi et al., 1996a) or suppressed ^{13}C NMR signals for certain residues (Saitô et al., 2000; Yamaguchi et al., 2000, 2001) due to interference with proton decoupling or magic angle spinning frequency (Rothwell and Waugh, 1981), respectively.

Paramagnetic ions such as Mn^{2+}, Gd^{3+} and stable free radicals have been used as relaxation reagents to determine interatomic distances in various molecular systems, including globular proteins in solution, by taking advantage of the effect of electron spin on relaxation times of nuclei in a distance-dependent manner (Chazin et al., 1987; Dwek, 1973; Jacob et al., 1999). We previously used Mn^{2+}, with ionic radius similar to that of Ca^{2+}, to locate the most

Received for publication 23 January 2001 and in final form 27 March 2001.

Address reprint requests to Dr. Hazime Saitô, Department of Life Science, Himeji Institute of Technology, Harima Science Garden City, Kouto 3-chome, Kamigori, Hyogo 678-1297, Japan. Tel.: +81-791-58-0181; Fax: +81-791-58-0182; E-mail: saito@sci.himeji-tech.ac.jp.

0006-3495/01/07/425/10 $2.00

probable binding sites for bR based on ^{13}C NMR change of [3-^{13}C]Ala-labeled bR (Tuzi et al., 1999), because the divalent cations have been proposed to be located at the membrane surfaces (Griffiths et al., 1996; Mitra and Stroud, 1990). We demonstrate here that combination of a series of site-directed replacements of Ala residues, together with selectively suppressed ^{13}C NMR peaks due to accelerated spin–spin relaxation rates caused by Mn^{2+} ions, are very useful to assign ^{13}C NMR signals of individual Ala residues located at the extracellular half of the transmembrane α-helices of membrane proteins. Further, it will be shown that the dynamic structure of such a region at ambient temperature is not always the same as that revealed by the x-ray diffraction studies (Luecke et al., 1999a; 2000) at lower temperature.

MATERIALS AND METHODS

[3-^{13}C]-L-alanine ([3-^{13}C]Ala) was purchased from Cambridge Isotope Laboratories, Inc. (Andover, MA) and used without further purification. The mutant strains of *H. salinarum*, A53V, D85N, and E204Q were provided by Prof. R. Needleman of Wayne State University and Prof. J. K. Lanyi of University of California, Irvine. The strains, A51G, A81G, A84G, A184G, P186A, and A215G were constructed as described by Needleman et al. (1991). *H. salinarum* strain S9 and the mutant strains were grown in the temporary synthetic (TS) medium (Onishi et al., 1965), in which unlabeled L-Ala was replaced by [3-^{13}C]Ala. The purple membranes containing bR were isolated and purified by the method of Oesterhelt and Stoeckenius (1974) and subsequently resuspended in 5 mM HEPES buffer (pH 7.0) containing 10 mM NaCl and 0.025% NaN_3. Mn^{2+} treatment of the purple membranes was carried out by resuspension of the membranes twice in 5 mM HEPES buffer (pH 7.0) containing 10 mM NaCl, 0.025% NaN_3 and 30–100 μM $MnCl_2$ to adjust final optical densities of chromophores to 1.00. The membranes thus prepared were finally concentrated by centrifugation and placed into a 5-mm outer diameter zirconia pencil-type NMR sample rotor for magic angle spinning and sealed tightly with glue to prevent evaporation of water.

High-resolution solid-state ^{13}C NMR spectra were recorded in the dark at 20°C on a Chemagnetics CMX-400 NMR spectrometer (Ft. Collins, CO) (^{13}C: 100.6 MHz), by cross-polarization—magic angle spinning (CP-MAS) and single-pulse excitation dipolar decoupled-magic angle spinning (DD-MAS) methods. The spectral width, acquisition time, and repetition time for CP-MAS and DD-MAS experiments were 40 kHz, 50 ms, and 4 s, respectively. The contact time for CP-MAS experiment was 1 ms. Free-induction decays were acquired with 2-K data points and Fourier-transformed as 8-K data points after 6-K data points were zero-filled. The $\pi/2$ pulses for carbon and proton were 5.0 μs and the spinning rates were 2.6 kHz. Resolution enhancement was performed by the method of Gaussian multiplication with apodization time 0 value of 0.7. Gaussian broadening value of 20 Hz was applied for the measurements of CP-MAS spectra of WT, D85N, A184G, P186A, A215G, and E204Q and 15 Hz was applied for those of A51G, A53V, A81G, and A84G to achieve an appropriate resolution. For DD-MAS spectra of WT, Gaussian broadening value of 12 Hz was applied. Transients were accumulated 6,000–24,000 times until a reasonable signal–noise ratio was achieved. The ^{13}C chemical shifts were referred to the carboxyl signal of glycine (176.03 ppm from tetramethylsilane (TMS)) and then expressed as relative shifts from the value of TMS.

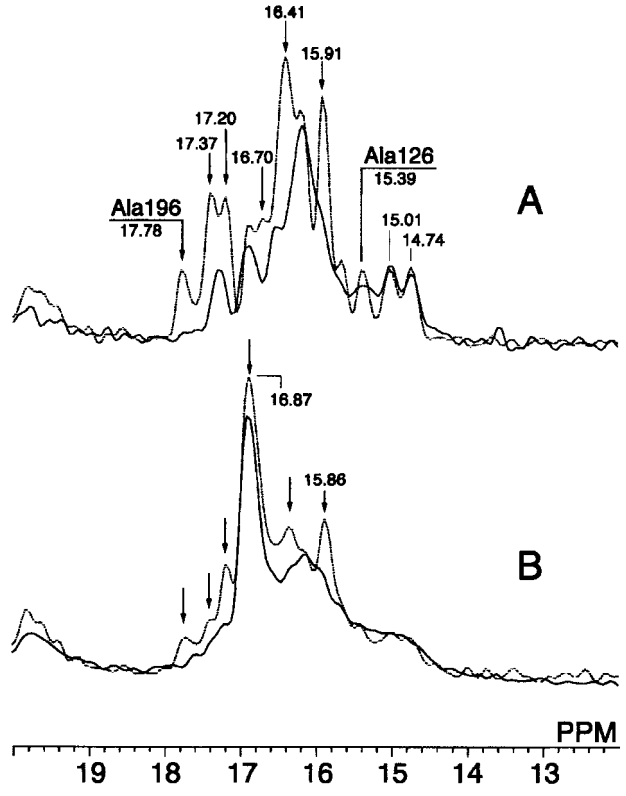

FIGURE 1 ^{13}C CP-MAS NMR spectra of [3-^{13}C]Ala-labeled wild-type bR in the presence (*A, solid trace*) and absence (*A, dotted trace*) of 30 μM Mn^{2+} ion, and ^{13}C DD-MAS NMR spectra of [3-^{13}C]Ala-labeled wild-type bR in the presence (*B, solid trace*) and absence (*B, dotted trace*) of 30 μM Mn^{2+} ion.

RESULTS

Figure 1 shows the ^{13}C (*A*) CP-MAS and (*B*) DD-MAS NMR spectra of wild-type bR in the presence of 30 μM Mn^{2+} ion. For the sake of comparison, the ^{13}C CP-MAS and DD-MAS spectra of bR in the absence of 30 μM Mn^{2+} (*dotted lines*) are superimposed. The peak-intensities for the ^{13}C NMR spectra with and without Mn^{2+} ion were normalized to adjust the highermost peaks, 14.74 and 15.01 ppm, whose intensities were not altered with or without Mn^{2+} ion. Several peaks, both from the CP-MAS and DD-MAS NMR spectra in the presence of Mn^{2+} ion as indicated by the arrows, were significantly suppressed from those without Mn^{2+} ion caused by accelerated relaxation pathways. In particular, the ^{13}C NMR peak of [3-^{13}C]Ala-196 signal, originally resonated at 17.78 ppm, is completely suppressed in the presence of Mn^{2+} ion, although the signals at 14.74 and 15.01 ppm were unchanged. This kind of differential broadening effect in the presence of Mn^{2+} ion should be ascribed to the extent of dipole–dipole interactions between Mn^{2+} and ^{13}C nuclei from individual residues. According to the Solomon–Bloembergen equation (Eq. 1), the magnitude of

the dipole–dipole interactions between the electron spin of Mn^{2+} and the ^{13}C nucleus is expressed as a function of distances between electron and nuclear spin (r) and correlation time of rotational reorientation of the spin pair (τ_r) (Bloembergen, 1957; Solomon, 1955),

$$\frac{1}{T_{2c}} = \frac{S(S+1)\gamma_c^2 g^2 \beta^2}{15r^6}\left(4\tau_{c1} + \frac{3\tau_{c1}}{1+\omega_c^2\tau_{c1}^2} + \frac{13\tau_{c2}}{1+\omega_e^2\tau_{c2}^2}\right) \quad (1)$$

$$\frac{1}{\tau_{c1}} = \frac{1}{T_{1e}} + \frac{1}{\tau_r} + \frac{1}{\tau_m} \qquad \frac{1}{\tau_{c2}} = \frac{1}{T_{2e}} + \frac{1}{\tau_r} + \frac{1}{\tau_m}$$

where T_{2C} is the spin–spin relaxation time of a ^{13}C nucleus, r is the distance between the ^{13}C nucleus and Mn^{2+}, S is the total electron spin, ω_c and ω_e are the nuclear and electronic Larmor precession frequencies, γ_c is the gyromagnetic ratio of ^{13}C, g is the g-factor of Mn^{2+}, β is the Bohr magneton, T_{1e} and T_{2e} are the spin–lattice and spin–spin relaxation times of an electron, τ_r is the rotational correlation time of the Mn^{2+}-bR complex and τ_m is the lifetime of the Mn^{2+}-bR complex. The g-factor and T_{1e} of Mn^{2+} is assumed to be identical to those of an aqua ion. τ_m is assumed to be longer than T_{1e} (3×10^{-9} s). When τ_r is longer than T_{1e}, the line width corresponding to the calculated T_{2C} value becomes greater than 100 Hz in the area within 8.7 Å of Mn^{2+}. This would be the case for the nuclei located at the transmembrane α-helices and short loops.

In Fig. 2, the areas within 8.7 Å from the carboxyl oxygen atoms in the potential cation binding sites, the acidic sidechains on the surfaces, and the previously proposed binding site at the C-terminus of the helix F, are shown by shaded area (Tuzi et al., 1999). The oxygens of the potential cation binding sites are shown by the large spheres, and the methyl carbons of Ala residues are shown by the small spheres with residue numbers. Here, the cation binding sites are assumed to be fully occupied by Mn^{2+}. This kind of the peak suppression is almost the same among concentrations of Mn^{2+} from 30 to 100 μM, as shown in Fig. 3. It is expected that most of the ^{13}C NMR signals of Ala residues located at the inner transmembrane α-helices, except for those at the interface residues, are unchanged in the spectra of Mn^{2+}-treated bRs. In the case of Ala residues with τ_r shorter than T_{1e}, as seen from the Ala residues undergoing rapid reorientational motions, the effect of Mn^{2+} on the line width is minimal depending on τ_r. This mechanism should explain why the peak at 16.87 ppm in the DD-MAS spectrum (Ala-240, 244, 245, and 246 located in the C-terminal random coil) is not broadened in spite of the presence of Mn^{2+} ion as shown in Fig. 1 *B*. In fact, τ_r of the C-terminal

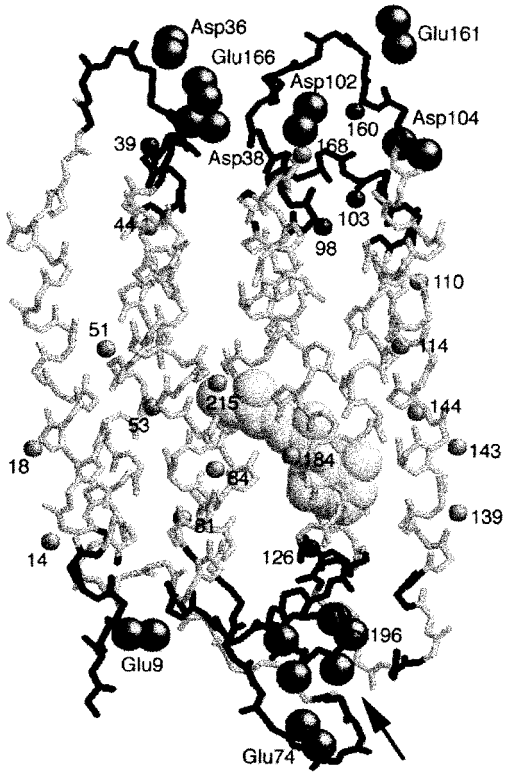

FIGURE 2 Atoms located within 8.7 Å from oxygens included in the potential cation binding sites (*large shaded spheres*) are shown by shaded areas. Sidechain methyl carbons of Ala residues are shown as small spheres with residue numbers. Previously proposed cation binding site at the C-terminus of the helix F is indicated by an arrow. The structure is from the coordinates proposed by the electron diffraction study by Mitsuoka et al.; 1999.

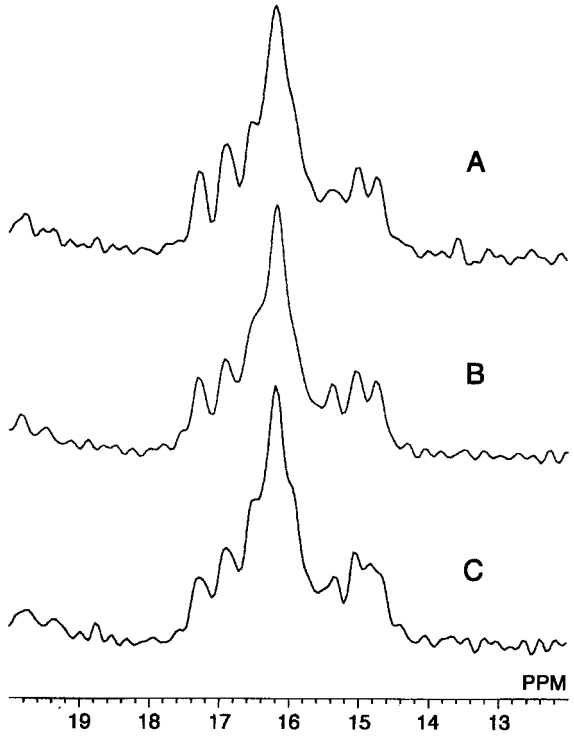

FIGURE 3 ^{13}C CP-MAS NMR spectra of [3-^{13}C]Ala-labeled wild-type bR in the presence of (*A*)30, (*B*) 40, and (*C*) 100 μM Mn^{2+} ion.

random coil should be shorter than 10^{-9} s, in contrast to the prolonged values for the C-terminal α-helix protruded from the membrane surface (10^{-6} s) resonated at 15.86 ppm (Yamaguchi et al., 2001). These findings are consistent with the previously proposed inhomogeneous distribution of mobility in the C-terminus of bR (Kawase et al., 2000; Renthal et al., 1983; Saitô et al., 2000; Tuzi et al., 1994; Yamaguchi et al., 1998, 2000, 2001).

To evaluate the effect of Mn^{2+} on the spectra of bR, influences of Mn^{2+} on a series of Ala residues around the extracellular half of the proton channel are assessed by examination of respective site-directed mutants by replacements of Ala by Gly or Val. Figure 4, *A* and *B*, show the ^{13}C CP-MAS NMR spectra of [3-^{13}C]Ala-labeled A215G and A81G mutants of bR, respectively. The top, middle, and bottom traces are the spectra of the site-directed mutants in the absence and presence of Mn^{2+} ion and the difference spectra between the wild type and mutant bRs in the presence of Mn^{2+} ion, respectively. For comparison, the dotted traces from the wild type were superimposed on the top and middle traces. As shown in Fig. 4 *A*, the peak from the difference spectrum at 16.20 ppm is unequivocally ascribed to the C_β signal of Ala-215, because no additional conformational change was accompanied by changing to this site-directed mutant. In a similar manner, the signals at 16.52 ppm is assigned to C_β signals of Ala-81 as shown in Fig. 4 *B*, although the accompanied dispersion signals arise from local conformational changes in the transmembrane α-helices induced by the replacement of Ala-81, present in a region between 14.8 and 16.2 ppm in the bottom traces. Among these dispersion signals, the pair of the simultaneous positive and negative peaks at 15.39 and 15.25 ppm in the bottom trace of Fig. 4 *B* are ascribed to the upfield displacement of the ^{13}C NMR peak of Ala-126 signal due to the accompanied local conformational change in A81G.

Figure 5, *A–C*, shows the ^{13}C CP-MAS NMR spectra of [3-^{13}C]Ala-labeled A184G in the absence and presence of Mn^{2+} ion and the difference spectrum between the wild type bR and A184G in the presence of Mn^{2+}, respectively. Figure 5 *D* shows the ^{13}C CP-MAS NMR spectrum of [3-^{13}C]Ala-labeled P186A in the presence of Mn^{2+} ion. For comparison, the dotted traces from the wild type were superimposed on Fig. 5, *A* and *B*. The replacement of Ala-184 by Gly causes the absence of the peak at 17.27 ppm and minor spectral changes in the higher field region in Fig. 5 *B*. The latter changes can be visualized as dispersion peaks representing displacements of signals caused by conformational changes in the difference spectrum (Fig. 5 *C*). The presence of the positive peak at 17.27 ppm in Fig. 5 *C*, which has no counterpart with the same magnitude of negative peak, is unequivocally assigned to Ala-184. Further, this assignment was confirmed by the fact that the Ala-184 signal at 17.27 ppm is displaced upfield by removal of kinked structure by replacement of Pro-186 with Ala (Fig. 5 *D*). This remarkable upfield displacement of the peak is ascribed to changes of the local torsion angles of peptide unit in Ala-184 located at the kink of the helix F induced by Pro-186, because the replacement of Pro-186 by Ala is

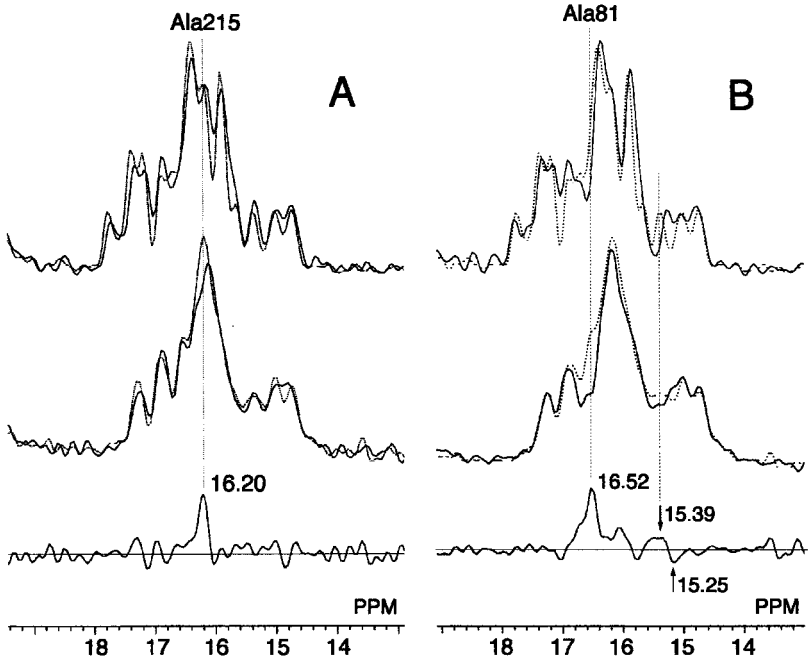

FIGURE 4 ^{13}C CP-MAS NMR spectra of [3-^{13}C]Ala-labeled (*A*) A215G and (*B*) A81G in the absence (*top solid traces*) and presence (*middle solid traces*) of Mn^{2+} ion. The corresponding spectra of [3-^{13}C]Ala-labeled wild-type bR are superimposed on the top and middle traces as dotted traces. Difference spectra between the spectra of the wild type and mutant bRs in the presence of Mn^{2+} ion are shown as the bottom traces.

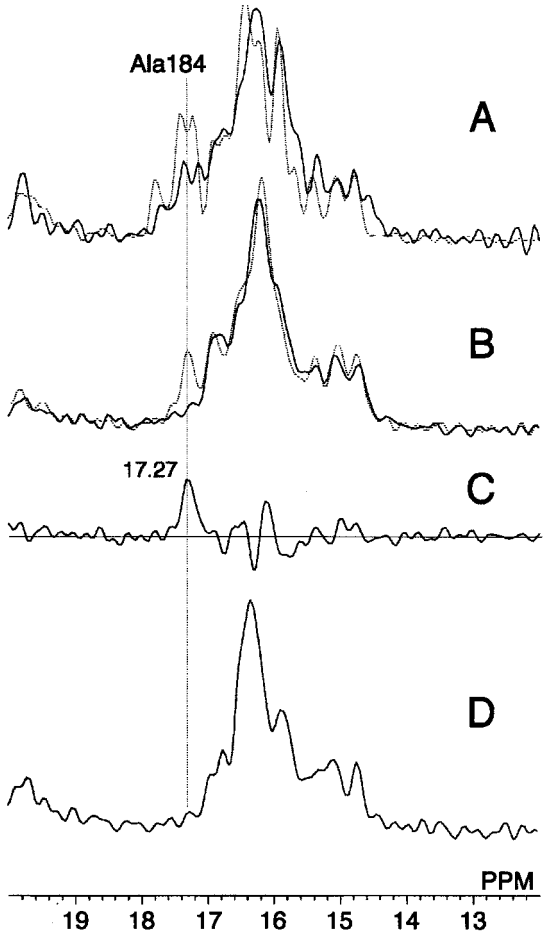

FIGURE 5 ^{13}C CP-MAS NMR spectra of [3-^{13}C]Ala-labeled A184G in the (*A*) absence and (*B*) presence of Mn^{2+} ion. The corresponding spectra of [3-^{13}C]Ala-labeled wild-type bR are superimposed as dotted traces. (*C*) Difference spectra between the spectra of the wild-type and mutant bRs in the presence of Mn^{2+} ion are shown as the bottom traces. (*D*) ^{13}C CP-MAS NMR spectra of [3-^{13}C]Ala-labeled P186A in the presence of Mn^{2+} ion.

expected to restore the kink to the normal α-helix and bring back the torsion angles of Ala-184 to those of the typical α-helix.

Figure 6, *A–C*, shows the ^{13}C CP-MAS NMR spectra of [3-^{13}C]Ala-labeled A51G, A53V, and A84G, respectively. The upper and lower traces are the spectra of the mutant bRs in the presence of Mn^{2+} ion and the difference spectra between the wild type and mutant bRs in the presence of Mn^{2+} ion, respectively. As shown in Fig. 6 *A*, the signal at 15.92 ppm in the difference spectra between the wild type and A51G is ascribed straightforwardly to Ala-51. The replacement of Ala-53 by Val induces changes of signals significantly larger than the noise level at 16.14, 15.95, and 15.46 ppm (Fig. 6 *B*). The pair of the positive and negative peaks at 15.95 and 15.46 ppm, respectively, is ascribed to the upfield displacement of the Ala-51 signal (15.92 ppm in Fig. 6 *A*) arising from an accompanied local conformational change at Ala-51 located near at Ala-53. Consequently, the remaining positive peak at 16.14 ppm is assigned straightforwardly to Ala-53. These assignments are in good agreement with the previous assignment based on wild-type bR and A53V (Tuzi et al., 1996b). A slight difference in the ^{13}C chemical shifts of the C_β signal of Ala-53 between the previously reported 16.3 ppm and the 16.14 ppm observed here may be attributed to the lower spectral resolution in the former. Figure 6 *C* shows that the peak from the difference spectrum at 16.89 ppm corresponding to the suppression of the peak at 16.89 ppm in the upper trace by about 50% is assigned to the C_β of Ala-84, consistent with the previous assignment (Yamaguchi et al., 2000). The remaining peak at 16.89 ppm has been assigned to Ala-240 of the C-terminus (Tanio et al., 1999). In addition, the positive peak at 16.52 ppm in the difference spectrum arises from the dispersion peak ascribed to the upfield shift of the Ala-81 signal originally resonated at 16.52 ppm. Also, positive and negative peaks around 16 ppm resemble those observed for A81G (*bottom trace* of Fig. 4 *B*), suggesting that the similar conformational changes in the transmembrane α-helices are induced by either the replacements of Ala-81 or Ala-84.

Potential application of this approach to detect function-related conformational change in the transmembrane region of membrane protein can be tested by using the local conformational change at the extracellular half of bR induced by the replacement of Glu-204 by Gln as shown in Fig. 7, *A* and *B*. The absence of the C_β signal of Ala-126 at 15.35 ppm induced by the replacement of Glu-204 was previously ascribed to the downfield displacement caused by the local conformational change in the extracellular surface of bR in the previous report (Tanio et al., 1999). In addition to this change, accompanied local conformational change at Ala-84 is obviously manifested from the upfield displacement of the C_β signal of Ala-84 in the Mn^{2+}-treated spectrum as shown in Fig. 7 *B*. In contrast, no spectral change at Ala-184 (17.27 ppm) is visible in spite of the replacement of Glu-204 (Fig. 7 *B*), suggesting that the local conformation at Ala-184 is unchanged between the wild type bR and E204Q. The downfield displacement of the most intense peak in the spectra of Mn^{2+}-treated bRs, from 16.14 to 16.37 ppm, is obviously induced by the replacement of Glu-204 (Fig. 7, *A* and *B*), suggesting the local conformational change of the transmembrane α-helices. Ala-53, originally resonated at 16.14 ppm, is likely to be included in this conformational change.

Figure 8, *C* and *D*, show the ^{13}C CP-MAS NMR spectra of D85N in the absence and presence of Mn^{2+}, respectively. Peak-intensities of the spectra in Fig. 8 *C* and *D* were normalized to adjust the heights of the peaks at 37.61 ppm arising from methylene carbons in the phytanyl group of lipid in the purple membrane. Mn^{2+} induces strong suppression of the whole spectrum of the Ala residues in D85N as shown in Fig. 8 *D*, which is not observed for the wild type bR (Fig. 8, *A* and *B*) and the other mutant bRs discussed here. The majority of the signal suppressions at

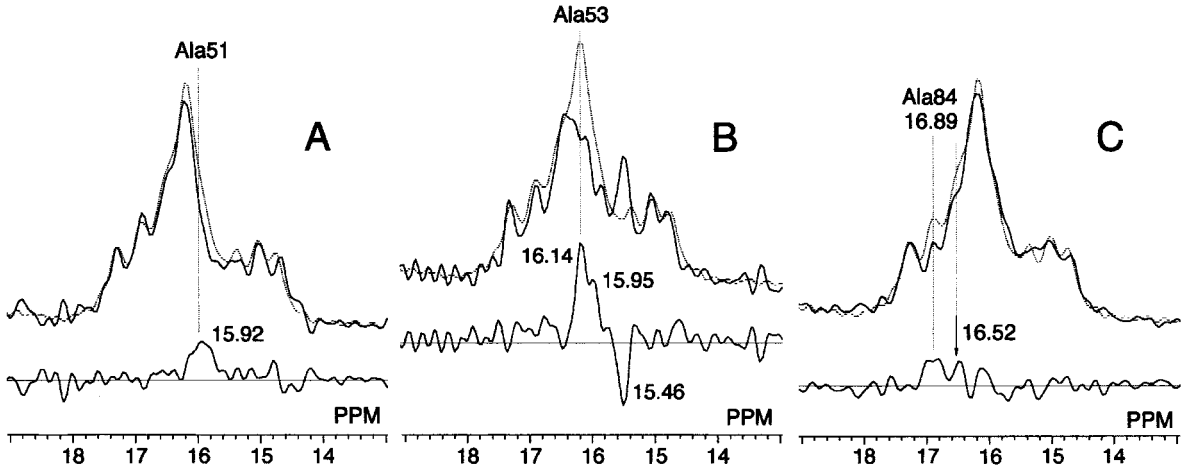

FIGURE 6 ^{13}C CP-MAS NMR spectra of [3-^{13}C]Ala-labeled (*A*) A51G, (*B*) A53G, and (*C*) A84G in the presence of Mn^{2+} ion (*upper solid traces*). The corresponding spectra of [3-^{13}C]Ala-labeled wild-type bR are superimposed on the top traces as dotted traces. Difference spectra between the spectra of the wild-type and mutant bRs in the presence of Mn^{2+} ion are shown as the bottom traces.

17.00, 17.36, and 17.54 ppm are ascribable to the suppressions of the signals from the loops located near at the water-accessible surface of D85N. In addition to the effect of Mn^{2+} on the loops, unexpectedly strong suppressions are observed for the peaks at 14.78, 15.04, 15.82, 16.34, and 16.60 ppm arising from the α-helices. The latter pronounced effect of Mn^{2+} about the suppressed peaks in D85N indicates that Mn^{2+} can penetrate more deeply into the inner transmembrane α-helices in D85N than in the wild type.

DISCUSSION

Editing the solid state ^{13}C NMR spectra of bR by Mn^{2+} ion

As described in the previous section, all of the ^{13}C NMR signals arising from the residues located at the extracellular half of bR, including Ala-51, 53, 81, 84, 184, 215, and 126 of bR, remain unchanged in the CP-MAS spectra in the presence of Mn^{2+} except for Ala-196. This finding is consistent with the estimated area where Mn^{2+} causes suppression of peak as shown in Fig. 2, except for Ala-126. This indicates that the area affected by Mn^{2+} is more restricted to the surface area than is our estimate, as shown in Fig. 2. It appears from the ^{13}C CP-MAS and DD-MAS NMR spectra of the wild-type and mutant bRs in the presence of Mn^{2+} (Figs. 1, 4, 5, and 6) that the two kinds of spectral changes are classified into the two groups: 1) unchanged signals from the hydrophobic transmembrane $\alpha-$helices and also from the C-terminal random coil, the latter of which undergoes rapid ($>10^9$ Hz) isotropic motion and is visible only in the DD-MAS spectra; 2) suppressed signals from the loops, α-helix termini and the C-terminal α-helix. It is noteworthy that the unambiguous assignments of the C_β ^{13}C NMR peaks of Ala-215 and Ala-184 are made possible in the presence of Mn^{2+} ion. It is emphasized that this approach can be easily extended to the other membrane protein–lipid bilayer systems, because low concentration of Mn^{2+} is expected to be locally distributed on the surface of a biomembrane containing negative charges from lipid head groups and acidic sidechains, without any serious perturbation to the system.

Dynamic structure of bR as viewed from Ala-215 and Ala-184 at ambient temperature

It is worthwhile to use the newly assigned signals, Ala-184 and Ala-215, as probes to show how the dynamic structure of the transmembrane region of bR at ambient temperature is modified from that revealed by diffraction studies at low temperature (Essen et al., 1998; Grigorieff et al., 1996; Kimura et al., 1997; Luecke, 2000; Luecke et al., 1999a; Mitsuoka et al., 1999; Pebay-Peyroula et al., 1997, 2000). The torsion angles of the peptide unit at Ala-184 are expected to be deviated substantially from those of the normal α-helices depending on the kink angle of the helix F, if any, because Ala-184 is shown to be located at the hinge of the kink of the helix F caused by a lack of hydrogen bond between the carbonyl oxygen of Trp-182 and the imido group of Pro-186. Consistent with this view, it was found that the ^{13}C chemical shift of C_β of Ala-184 is resonated at the unusually lower field region at 17.27 ppm as a residue belonging to the transmembrane α-helices. This is probably because Ala-184 takes highly distorted torsion angles that are either static or time-averaged. This observation is consistent with the previous prediction by x-ray structure [$(\phi, \psi) = (-75°, -24°)$ (Luecke et al., 1999a)]. This view is also justified because the ^{13}C signal of Ala C_β at Ala-184 was dis-

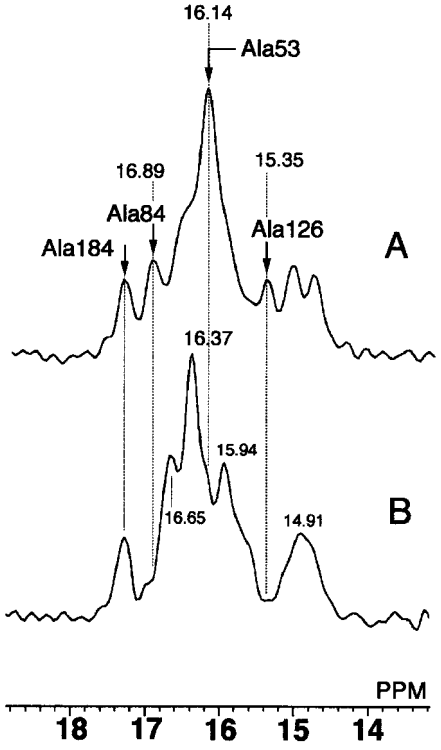

FIGURE 7 ^{13}C CP-MAS NMR spectra of [3-^{13}C]Ala-labeled wild-type (*A*) bR and (*B*) E204Q in the presence of Mn^{2+}.

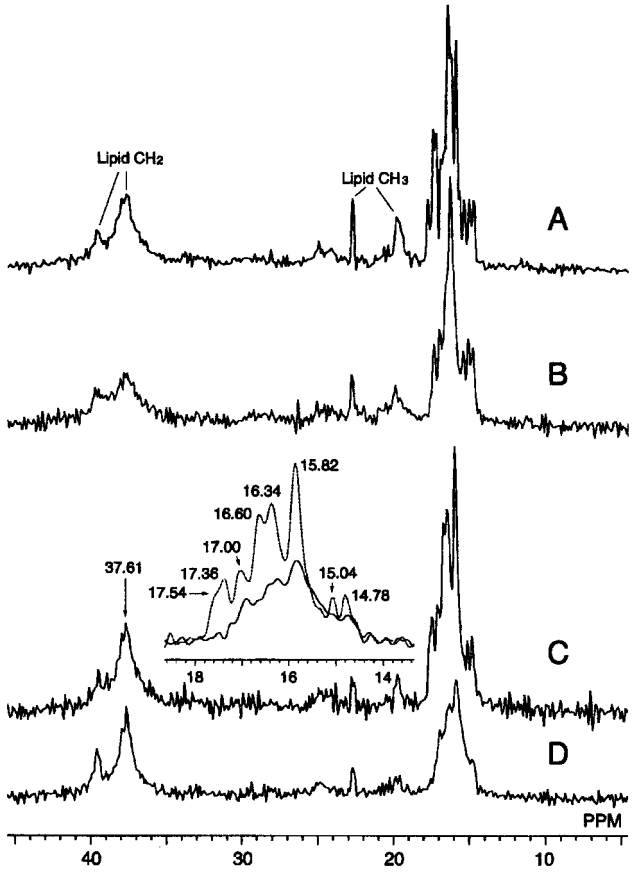

FIGURE 8 ^{13}C CP-MAS NMR spectra of [3-^{13}C]Ala-labeled wild-type bR in the (*A*) absence and (*B*) presence of Mn^{2+} ion, and ^{13}C CP-MAS NMR spectra of [3-^{13}C]Ala-labeled D85N in the (*C*) absence and (*D*) presence of Mn^{2+} ion. Expanded spectra of D85N in the absence (*dotted trace*) and presence (*solid trace*) of Mn^{2+} ion are shown as an inset.

placed upfield toward the peak position of the normal α-helix, when this kinked structure in the helix F is removed by mutation of Pro186 → Ala (Fig. 5 *D*). Therefore, it is possible to use this Ala C_β ^{13}C NMR peak of Ala-184 as a suitable probe to examine the kinked structure at the transmembrane helix F. Ala-215, neighbored to Lys-216 and forming the Schiff base linkage with retinal, has been shown to be involved in the π-bulge as clarified by the x-ray study (Luecke et al., 1999a). Local torsion angles for the peptide unit at Ala-215 were shown to be $(\phi, \psi) = (-77°, -16°)$, substantially deviated from those of the typical $\alpha-$helix, $(\phi, \psi) = (-57°, -47°)$ to the direction similar to Ala-184 $[(\phi, \psi) = (-75°, -24°)]$. Downfield displacement of the ^{13}C chemical shift of Ala-215 from that of the normal α-helix can be expected from the ^{13}C NMR chemical shift contour map for C_β carbon of Ala based on quantum-chemical calculation (Ando et al., 1998), in view of the displacement of the observed peak for Ala-184. In contrast to the expectation, the observed ^{13}C chemical shift for the Ala C_β of Ala-215 at 16.2 ppm is rather normal as the α-helix comparable to the data of Ala-53 and Ala-51, both of which are located at the typical α-helix structure in the transmembrane helix B. As pointed out, Ala C_β ^{13}C chemical shift of polypeptides and proteins is determined by the torsion angles (ϕ, ψ) (Saitô, 1986; Saitô and Ando, 1989) as long as the residue under consideration is static. Therefore, it is more likely that Ala-215 takes the typical α-helix rather than the π-bulge, at least at ambient temperature, based on the above-mentioned similarity of the ^{13}C chemical shifts among Ala-215, Ala-53, and Ala-51. It is plausible as a cause for this discrepancy that bR here for NMR measurement is embedded in the purple membrane as 2D crystal suspended in the buffer at 20°C, although many x-ray diffractions have been performed at lower temperature, such as liquid nitrogen temperature together with 3D crystal. The presence of slow conformational fluctuation in the transmembrane α-helices of bR with a frequency of 100 Hz at ambient temperature, and freezing of this motion at temperature below −40°C were observed by the solid state ^{13}C NMR (Tuzi et al., 1996a). The neutron-scattering studies at ambient temperature also showed a large amplitude anharmonic motion of bR in the purple membrane with a frequency in the region of 10^9 to 10^{14} Hz (Ferrand et al., 1993; Fitter et al., 1998; Heberle et al., 2000). A possible change in the time-averaged torsion angles induced by these motions, if any, would result in displacement of ^{13}C chemical shift of Ala,

because the conformation-dependent ^{13}C NMR chemical shift of C_β of Ala turned out to be sensitive to the dynamically averaged torsion angles (Kimura et al., 2001) if an Ala residue is involved in local conformational fluctuation at a frequency higher than 10^2 Hz. Therefore, dynamic behavior of bR at ambient temperature might permit more relaxed conformation of the backbone around Ala-215 than that under the lower temperature.

Detection of the time-averaged conformational change in the proton channel

It is now demonstrated that detailed examination for local conformational changes is made possible by using Mn^{2+} as relaxation reagent to simplify spectral pattern, even if signals under consideration are accidentally superimposed with signals of other residues. For instance, the C_β ^{13}C NMR peak of Ala-84 of wild type bR resonated at 16.89 ppm is displaced upfield at least by 0.24 ppm when the ^{13}C NMR spectrum of E204Q was compared (Fig. 7). This is because local backbone conformation at the helix C near Asp-85, the proton acceptor of the early half of the photo reaction, is changed by replacement of the side-chain of Glu-204 included in the proton release site located at the extracellular surface. In addition, the most intense peak at 16.14 ppm is displaced downfield to 16.37 ppm, presumably reflecting an accompanied conformational change at Ala-53 originally resonated at 16.14 ppm, together with the conformational change of the helix B near the Schiff base and Asp-85. The well-known linkage of the pKa of Asp-85 with the proton-releasing groups, which is proposed to contribute to the stabilization of the protonated Asp-85 during the formation of the M-intermediate, has been reported to be modified by the replacement of Glu-204 with Gln (Richter et al., 1996). Even at the ground state, the two apparent pKa of Asp-85 in the wild-type bR is changed into the single pKa in E204Q. Interestingly, no conformational difference between the wild type and E204Q in the region near the retinal have been observed in the x-ray model structures for the ground state at low temperature (Luecke et al., 2000). Actually, the backbone torsion angles of Ala-84 [$(\phi, \psi) = (-64°, -38°)$] and Ala-53 [$(\phi, \psi) = (-61°, -36°)$] in the model structure of E204Q are virtually identical to those in the wild type, $(\phi, \psi) = (-63°, -36°)$ and $(-64°, -37°)$, respectively. Consequently, the differences between the backbone conformation of the wild type and E204Q obviously detected by ^{13}C NMR should be ascribed to differences in dynamically averaged conformations at ambient temperature deviated from the static conformation observed at low temperature by thermal motions. The remarkable changes in the dynamically averaged backbone conformation in the region near Asp-85 and the Schiff base would be responsible for the change in the pKa coupling between Asp-85 and the proton-releasing groups at the ground state, although the reported less dramatic changes of the Ala-82 sidechain and water (Wat-406) in the x-ray model structure of E204Q might also participate in the change of the pKa coupling. The interaction between Asp-85 and the proton-releasing groups mediated by changes of the dynamically averaged conformations might be also required during the photoreaction of bR as a pKa-controlling mechanism for stabilization of the protonated Asp-85 in the M-intermediate. On the contrary, the unchanged peak position of the ^{13}C NMR peak of C_β Ala-184 between wild type and E204Q indicate that the possible conformational change due to the kink in the helix F is not influenced by the change at Glu-204, although distance between Ala-184 and Glu-204 is shorter than that between Ala-84 and Glu-204 in x-ray structure. Thus, the influence of the replacement of Glu-204 should be spatially restricted to the structure around the proton channel.

In contrast to the spatially restricted influence of Mn^{2+} on the spectra of the wild type bR, E204Q and other Ala-replaced mutant bRs, the effect of Mn^{2+} on the spectra of D85N is less specific and causes decrease in the intensity of whole spectrum of D85N. The strong suppression of the peaks arising from the α-helices in D85N suggests the increase of the Mn^{2+} accessibility to the inner transmembrane moiety or lipid-protein interface of bR. This is consistent with the previously reported large conformational change of the transmembrane α-helices at neutral pH induced by the replacement of Asp-85 by Asn (Kawase et al., 2000). This conformational change might cause continuous or transient opening of the proton channel that facilitates the access of Mn^{2+} to the transmembrane α-helices surrounding the proton channel, or distortion of molecular packing of bRs and lipids in the purple membrane, which facilitates the access of Mn^{2+} to the hydrophobic outside surface of bR.

The authors are grateful to Professors Richard Needleman and Janos K. Lanyi for providing A53V, D85N, and E204Q mutant strains of *H. Salinarum*.

This work has been supported in part by Grants-in-Aid for Scientific Research (11780476) from the Ministry of Education, Science, Sports, and Culture of Japan.

REFERENCES

Ando, I., N. Asakawa, and G. A. Webb. 1998. NMR chemical shift and electronic structure. *In* Solid State NMR of Polymers. I. Ando and T. Asakura, editors. Elsevier, Amsterdam. 1–21.

Bloembergen, N. 1957. Proton relaxation times in paramagnetic solutions. *J. Chem. Phys.* 27:572–573.

Chazin, W. J., M. Rance, and P. E. Wright. 1987. Complete assignment of lysine resonances in ^1H NMR spectra of proteins as probes of surface structure and dynamics. *FEBS Lett.* 222:109–114.

Cross, T. A. 1997. Solid-state nuclear magnetic resonance characterization of gramicidin channel structure. *Methods Enzymol.* 289:672–696.

Dwek, A. D. 1973. Nuclear Magnetic Resonance in Biochemistry: Applications to Enzyme Systems. W. Harrington, and A. R. Peacocke, editors. Oxford University Press, London. 174–246.

Edman, K., P. Nollert, A. Royant, H. Belrhali, P. E. Pebay, J. Hajdu, R. Neutze, and E. M. Landau. 1999. High-resolution x-ray structure of an early intermediate in the bacteriorhodopsin photocycle. *Nature.* 401: 822–826.

Essen, L. O., R. Siegert, W. D. Lehmann, and D. Oesterhelt. 1998. Lipid patches in membrane protein oligomers: crystal structure of the bacteriorhodopsin–lipid complex. *Proc. Natl. Acad. Sci. U.S.A.* 95: 11673–11678.

Ferrand, M., A. J. Dianoux, W. Petry, and G. Zaccai. 1993. Thermal motions and function of bacteriorhodopsin in purple membranes: effects of temperature and hydration studied by neutron scattering. *Proc. Natl. Acad. Sci. U.S.A.* 90:9668–9672.

Fitter, J., S. A. Verclas, R. E. Lechner, H. Seelert, and N. A. Dencher. 1998. Function and picosecond dynamics of bacteriorhodopsin in purple membrane at different lipidation and hydration. *FEBS Lett.* 433: 321–325.

Griffiths, J. A., J. King, D. Yang, R. Browner, and M. A. El-Sayed. 1996. Calcium and magnesium binding in native and structurally perturbed purple membrane. *J. Phys. Chem.* 100:929–933.

Grigorieff, N., T. A. Ceska, K. H. Downing, J. M. Baldwin, and R. Henderson. 1996. Electron-crystallographic refinement of the structure of bacteriorhodopsin. *J. Mol. Biol.* 259:393–421.

Heberle, J., J. Fitter, H. J. Sass, and G. Buldt. 2000. Bacteriorhodopsin: the functional details of a molecular machine are being resolved. *Biophys. Chem.* 85:229–248.

Jacob, J., B. Baker, R. G. Bryant, and D. S. Cafiso. 1999. Distance estimates from paramagnetic enhancements of nuclear relaxation in linear and flexible model peptides. *Biophys. J.* 77:1086–1092.

Kawase, Y., M. Tanio, A. Kira, S. Yamaguchi, S. Tuzi, A. Naito, M. Kataoka, J. K. Lanyi, R. Needleman, and H. Saitô. 2000. Alteration of conformation and dynamics of bacteriorhodopsin induced by protonation of Asp 85 and deprotonation of Schiff base as studied by ^{13}C NMR. *Biochemistry.* 39:14472–14480.

Kimura, S., A. Naito, S. Tuzi, and H. Saitô. 2001. A ^{13}C NMR study on [3-^{13}C]-, [1-^{13}C]Ala-, or [1-^{13}C]Val-labeled transmembrane peptides of bacteriorhodopsin in lipid bilayers: insertion, rigid-body motions, and local conformational fluctuations at ambient temperature. *Biopolymers.* 58:78–88.

Kimura, Y., D. G. Vassylyev, A. Miyazawa, A. Kidera, M. Matsushima, K. Mitsuoka, K. Murata, T. Hirai, and Y. Fujiyoshi. 1997. Surface of bacteriorhodopsin revealed by high-resolution electron crystallography. *Nature.* 389:206–211.

Lanyi, J. K. 1993. Proton translocation mechanism and energetics in the light-driven pump bacteriorhodopsin. *Biochim. Biophys. Acta.* 1183: 241–246.

Lanyi, J. K. 1997. Mechanism of ion transport across membranes. Bacteriorhodopsin as a prototype for proton pumps. *J. Biol. Chem.* 272: 31209–31212.

Luecke, H. 2000. Atomic resolution structures of bacteriorhodopsin photocycle intermediates: the role of discrete water molecules in the function of this light-driven ion pump. *Biochim. Biophys. Acta.* 1460: 133–156.

Luecke, H., B. Schobert, J. P. Cartailler, H. T. Richter, A. Rosengarth, R. Needleman, and J. K. Lanyi. 2000. Coupling photoisomerization of retinal to directional transport in bacteriorhodopsin. *J. Mol. Biol.* 300: 1237–1255.

Luecke, H., B. Schobert, H. T. Richter, J. P. Cartailler, and J. K. Lanyi. 1999a. Structure of bacteriorhodopsin at 1.55 Å resolution. *J. Mol. Biol.* 291:899–911.

Luecke, H., B. Schobert, H. T. Richter, J. P. Cartailler, and J. K. Lanyi. 1999b. Structural changes in bacteriorhodopsin during ion transport at 2 angstrom resolution. *Science.* 286:255–261.

Marassi, F. M., and S. J. Opella. 1998. NMR structural studies of membrane proteins. *Curr. Opin. Struct. Biol.* 8:640–648.

Mathies, R. A., S. W. Lin, J. B. Ames, and W. T. Pollard. 1991. From femtoseconds to biology: mechanism of bacteriorhodopsin's light-driven proton pump. *Annu. Rev. Biophys. Chem.* 20:491–518.

Mitra, A. K., and R. M. Stroud. 1990. High sensitivity electron diffraction analysis. A study of divalent cation binding to purple membrane. *Biophys. J.* 57:301–311.

Mitsuoka, K., T. Hirai, K. Murata, A. Miyazawa, A. Kidera, Y. Kimura, and Y. Fujiyoshi. 1999. The structure of bacteriorhodopsin at 3.0 Å resolution based on electron crystallography: implication of the charge distribution. *J. Mol. Biol.* 286:861–882.

Needleman, R., M. Chang, B. Ni, G. Varo, J. Fornes, S. H. White, and J. K. Lanyi. 1991. Properties of Asp212—Asn bacteriorhodopsin suggest that Asp212 and Asp85 both participate in a counterion and proton acceptor complex near the Schiff base. *J. Biol. Chem.* 266:11478–11484.

Oesterhelt, D., and W. Stoeckenius. 1974. Isolation of the cell membrane of *Halobacterium halobium* and its fractionation into red and purple membrane. *Methods Enzymol.* 31:667–678.

Onishi, H., M. E. McCance, and N. E. Gibbons. 1965. A synthetic medium for extremely halophilic bacteria. *Can. J. Microbiol.* 11:365–373.

Ovchinnikov, Y. 1982. Rhodopsin and bacteriorhodopsin: structure–function relationships. *FEBS. Lett.* 148:179–191.

Pebay-Peyroula, E., R. Neutze, and E. M. Landau. 2000. Lipidic cubic phase crystallization of bacteriorhodopsin and cryotrapping of intermediates: towards resolving a revolving photocycle. *Biochim. Biophys. Acta.* 1460:119–132.

Pebay-Peyroula, E., G. Rummel, J. P. Rosenbusch, and E. M. Landau. 1997. X-ray structure of bacteriorhodopsin at 2.5 angstroms from microcrystals grown in lipidic cubic phases. *Science.* 277:1676–1681.

Renthal, R., N. Dawson, J. Tuley, and P. Horowitz. 1983. Constraints on the flexibility of bacteriorhodopsin's carboxyl-terminal tail at the purple membrane surface. *Biochemistry.* 22:5–12.

Richter, H.-T., L. S. Brown, R. Needleman, and J. K. Lanyi. 1996. A linkage of the pK_a's of asp-85 and glu-204 forms part of the reprotonation switch of bacteriorhodopsin. *Biochemistry.* 35:4054–4062.

Rothwell, W. P., and J. S. Waugh. 1981. Transverse relaxation of dipolar coupled spin systems under rf irradiation: Detecting motions in solid. *J. Chem. Phys.* 75:2721–2732.

Saitô, H. 1986. Conformation-dependent ^{13}C chemical shifts: a new means of conformational characterization as obtained by high-resolution solid-state NMR. *Magn. Reson. Chem.* 24:835–852.

Saitô, H., and I. Ando. 1989. High-resolution solid-state NMR studies of synthetic and biological macromolecules. *Annu. Rep. NMR Spectrosc.* 21:209–290.

Saitô, H., S. Tuzi, and A. Naito. 1998. Empirical vs. nonempirical evaluation of secondary structure of fibrous and membrane proteins. *Annu. Rep. NMR Spectrosc.* 36:79–121.

Saitô, H., S. Tuzi, S. Yamaguchi, M. Tanio, and A. Naito. 2000. Conformation and backbone dynamics of bacteriorhodopsin revealed by ^{13}C-NMR. *Biochim. Biophys. Acta.* 1460:39–48.

Sass, H. J., G. Buldt, R. Gessenich, D. Hehn, D. Neff, R. Schlesinger, J. Berendzen, and P. Ormos. 2000. Structural alterations for proton translocation in the M state of wild-type bacteriorhodopsin. *Nature.* 40: 649–653.

Solomon, I. 1955. Relaxation processes in a system of two spins. *Phys. Rev.* 99:559–565.

Stoeckenius, W., and R. A. Bogomolni. 1982. Bacteriorhodopsin and related pigments of *Halobacteria*. *Annu. Rev. Biochem.* 52:587–616.

Tanio, M., S. Tuzi, S. Yamaguchi, R. Kawaminami, A. Naito, R. Needleman, J. K. Lanyi, and H. Saitô. 1999. Conformational changes of bacteriorhodopsin along the proton-conduction chain as studied with ^{13}C NMR of [3-^{13}C]Ala-labeled protein: Arg^{82} may function as an information mediator. *Biophys. J.* 77:1577–1584.

Tuzi, S., A. Naito, and H. Saitô. 1994. ^{13}C NMR study on conformation and dynamics of the transmembrane α-helices, loops, and C-terminus of [3-^{13}C]Ala-labeled bacteriorhodopsin. *Biochemistry.* 33:15046–15052.

Tuzi, S., A. Naito, and H. Saitô. 1996a. Temperature-dependent conformational change of bacteriorhodopsin as studied by solid-state ^{13}C NMR. *Eur. J. Biochem.* 239:294–301.

Tuzi, S., S. Yamaguchi, A. Naito, R. Needleman, J. K. Lanyi, and H. Saitô. 1996b. Conformation and dynamics of [3-^{13}C]Ala- labeled bacteriorhodopsin and bacterioopsin, induced by interaction with retinal and its

analogs, as studied by ^{13}C nuclear magnetic resonance. *Biochemistry.* 35:7520–7527.

Tuzi, S., S. Yamaguchi, M. Tanio, H. Konishi, S. Inoue, A. Naito, R. Needleman, J. K. Lanyi, and H. Saitô. 1999. Location of a cation-binding site in the loop between helices F and G of bacteriorhodopsin as studied by ^{13}C NMR. *Biophys. J.* 76:1523–1531.

Yamaguchi, S., S. Tuzi, T. Seki, M. Tanio, R. Needleman, J. K. Lanyi, A. Naito, and H. Saitô. 1998. Stability of the C-terminal α-helical domain of bacteriorhodopsin that protrudes from the membrane surface, as studied by high-resolution solid-state ^{13}C NMR. *J. Biochem. (Tokyo).* 123:78–86.

Yamaguchi, S., S. Tuzi, M. Tanio, A. Naito, J. K. Lanyi, R. Needleman, and H. Saitô. 2000. Irreversible conformational change of bacterio-opsin induced by binding of retinal during its reconstitution to bacteriorhodopsin, as studied by ^{13}C NMR. *J. Biochem. (Tokyo).* 127:861–869.

Yamaguchi, S., K. Yonebayashi, H. Konishi, S. Tuzi, A. Naito, J. K. Lanyi, R. Needleman, and H. Saitô. 2001. Cytoplasmic surface structure of bacteriorhodopsin consisting of interhelical loops and C-terminal α-helix, modified by a variety of environmental factors as studied by ^{13}C NMR. *J. Biochem. (Tokyo).* 129:373–382.